Assessment of Dynamical Downscaling in Near-Surface Fields with Different Spectral Nudging Approaches Using the Nested Regional Climate Model (NRCM)

JIALI WANG AND VEERABHADRA R. KOTAMARTHI

Environmental Science Division, Argonne National Laboratory, Argonne, Illinois

(Manuscript received 5 November 2012, in final form 8 January 2013)

ABSTRACT

Dynamic downscaling with regional-scale climate models is used widely for increasing the spatial resolution of global-scale climate model projections. One uncertainty in generating these projections is the choice of boundary forcing applied. In this study the Nested Regional Climate Model (NRCM) is used with a grid spacing of 12 km over the United States (excluding Hawaii) to dynamically downscale 2.5° National Centers for Environmental Prediction–U.S. Department of Energy Reanalysis-2 data, with different applications of spectral nudging (SN) for the boundary conditions. Nine numerical experiments for July 2005—each with different wavenumbers and nudging duration periods, applied to different model layers—evaluated the performance of SN in downscaling near-surface fields. The calculations were compared with the North America Regional Reanalysis dataset over four subregions of the contiguous 48 states. Results show significant differences with different wavenumbers, nudging duration periods, and nudging altitudes. The short-period SN with three waves, applied above 850 hPa, showed the highest skill in simulating precipitation, whereas whole-period SN produced a higher skill level and performed slightly better than short-period SN for surface temperature and 10-m wind, respectively. Differences in the performance of SN applied at different altitudes were not significant. On the basis of the comparisons for precipitation, surface temperature, and wind fields over entire contiguous states, whole-period nudging with six waves starting above 850 hPa for downscaling calculations for climate-related variables is recommended. This method improved the performance of the NRCM in predicting near-surface fields by more than 30.5% relative to a case with no nudging.

1. Introduction

When considering the impacts of global climate change due to increases in the atmospheric concentration of carbon dioxide (Houghton et al. 1990, 1992, 1996) and other trace gases, the focus is primarily on impacts at the local and regional scales resulting from large-scale changes (e.g., Wilby et al. 1998; Civerolo et al. 2008). Although general circulation models (GCMs) demonstrate significant skill at the continental and hemispheric spatial scales and incorporate a large proportion of the complexity of the global system, they are inherently unable to represent local subgrid-scale features and dynamics because of their coarse resolutions (Wigley et al. 1990; Carter et al. 1994). Thus, the need for a downscaling methodology was recognized. Two common methods, dynamical downscaling and statistical downscaling, have filled this gap with varying degrees of success. The dynamic downscaling methodology, developed by using existing regional-scale numerical weather prediction models (Giorgi 2006; Mearns 2009), has become a common approach for obtaining high-resolution regional climate information from GCMs.

However, it is a challenge to balance the performance of regional climate models (RCMs) in adding small-scale features while simultaneously retaining large-scale features (Liu et al. 2012). Most RCMs have systematic errors associated with uncertainties in their dynamics, physical parameterization, boundary conditions, initialization, and domain choice, as well as the resolution of the numerical models (Giorgi and Mearns 1999; Liang et al. 2001; Miguez-Macho et al. 2005; Lo et al. 2008; Caldwell et al. 2009). One key source of dynamical downscaling error is inconsistency along boundaries, because over time RCM simulation starts deviating from the GCMs, driving

Corresponding author address: V. R. Kotamarthi, Environmental Science Division, Bldg. 203, J101, Argonne National Laboratory, 9700 South Cass Ave., Argonne, IL 60439-4843.
E-mail: vrkotamarthi@anl.gov

DOI: 10.1175/JAMC-D-12-0302.1

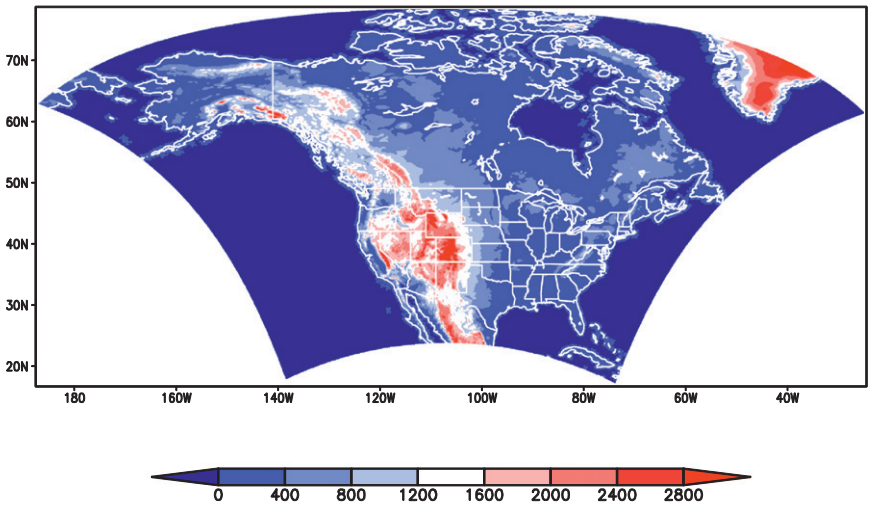

FIG. 1. NRCM model domain and topography map. Color scale refers to elevations (m).

fields that are imposed at the boundaries (Davies 1976, 1983). Nudging techniques (methods for adding a correction to the predictive equation of the variable to be adjusted at each grid point in the model) have proved useful for preventing RCMs from drifting away from the large-scale dynamics (Mabuchi et al. 2002; Miguez-Macho et al. 2005; Lo et al. 2008). Two kinds of nudging techniques are widely employed: 1) brute-force grid nudging conducted in every grid cell (Stauffer and Seaman 1990) and 2) spectral nudging (SN) applied in the zonal and meridional directions. Only the waves under a selected wavenumber, chosen to be representative of large-scale forcing, are kept in the nudging term (Waldron et al. 1996; von Storch et al. 2000; Miguez-Macho et al. 2004; 2005). A number of studies have shown that SN has an advantage over no-nudging or boundary relaxation techniques (Feser 2006; Feser and von Storch 2005; Rockel et al. 2008). Miguez-Macho et al. (2004) showed that SN successfully eliminated the distortion of the spatial pattern of precipitation when the position of the simulation domain was shifted by 7°–17°. Liu et al. (2012) compared the performance of grid nudging and SN in downscaling with the Weather Research and Forecasting (WRF) model and found that SN outperformed grid nudging in balancing the performance of the simulation at large and small scales.

This study aimed to assess the performance of different SN approaches in dynamical downscaling of the National Centers for Environmental Prediction (NCEP)–U.S. Department of Energy Reanalysis-2 (R-2) dataset with the Nested Regional Climate Model (NRCM), a version of the WRF model (Holland et al. 2010). We will answer the following questions: 1) When dynamical downscaling is conducted with NRCM, what are the effects of nudging at different wavenumbers, durations, and lowest altitudes of application on the performance of SN in near-surface fields? 2) How well do these different approaches perform over distinct subregions of the contiguous United States?

Section 2 of this paper provides an overview of the model setup, the SN methods as applied to the NRCM model, and the experimental designs with the SN technique. Section 3 presents results for the experiments with different SN techniques, verifies the performance of different experiments in near-surface fields with statistical approaches over distinct subregions, and ranks the performance of the various SN techniques. A summary and a discussion of uncertainties of the model are in section 4.

2. Model setup and experiments with spectral nudging

a. Model setup

The NRCM used in this study is the WRF model with the Advanced Research WRF dynamic core, version 3.3.1. In this version, sea surface temperature (SST) is updated every 6 h, and a diurnal signal added to skin SST provides a more accurate lower-boundary condition. The simulation domain centered at 52.24°N and 105.5°W and with dimensions of 600 × 516 horizontal grids points and spacing of 12 km, covered the contiguous United States (CONUS), Alaska, and most parts of Canada and northern Mexico (Fig. 1). The Lambert conformal conic projection was used. The vertical dimension comprised 50 terrain-following eta levels. The pressure at the top of the model was 100 hPa. Initial

and boundary conditions for the large-scale atmospheric fields, as well as initial soil parameters (soil water, moisture, and temperature), were given by the 6-h, 2.5° × 2.5° R-2 data, and SST values were given by the daily and 0.5° × 0.5° NCEP global analysis. The domain-specified lateral boundary was composed of a one-point specified zone and a nine-point relaxation zone (Davies and Turner 1977), and the nine-point relaxation zone was set up according to the suggestion by Giorgi et al. (1993) that larger relaxation zones can reduce noise generation at the boundaries.

The main physical options we used include the WRF single-moment six-class (WSM6) microphysical parameterization (Hong and Lim 2006), Dudhia shortwave radiation (Dudhia 1989), Rapid Radiative Transfer Model longwave radiation (Mlawer et al. 1997), the Yonsei University planetary boundary layer (PBL) scheme (Noh et al. 2003), and the Noah land surface model (Chen and Dudhia 2001). The Grell–Devenyi ensemble scheme (Grell et al. 1994) was employed, because it performed better in the spatial distribution of precipitation than the newer Kain–Fritsch convective scheme (Kain 2004) over the domain for July 2005 in this study. We also updated the deep-layer soil temperature, a necessary input for long simulations (Wang et al. 2012).

The model was integrated from 0000 UTC 30 June to 0000 UTC 31 July 2005. The initial 24 h was considered a spinup period, and the outputs during this period were excluded from the analysis. The evaluation period was from 0000 UTC 1 July to 0000 UTC 31 July 2005, and the verification region covered CONUS, excluding oceans and lakes. The 32-km NCEP North American Regional Reanalysis (NARR) dataset was used for model validation. The quality of the NARR data was evaluated with surface station and sounding measurements of Mesinger et al. (2006). The similarities in temperature and wind component between NARR and NCEP–National Center for Atmospheric Research (NCAR) reanalysis data were found to be very high at large scales by Liu et al. (2012). We have evaluated the NARR precipitation with the Tropical Rainfall Measuring Mission (TRMM) 3B43 dataset as a part of this study (not shown), and we found the agreement to be high over the entire CONUS except over parts of southern California, which is marked by very low rainfall for the period used for evaluation. Thus, NARR data can be viewed as a reasonable criterion to verify the downscaled results from NCEP–NCAR data.

b. Spectral nudging methods

Originally introduced for a regional model by Waldron et al. (1996), SN has also been applied for climate simulations by von Storch et al. (2000). The SN technique is based on the fact that small-scale features in model-calculated fields result from an interplay between larger-scale atmospheric flow and smaller-scale geographic features such as topography, land–sea distribution, or land use (von Storch 1999). To describe these small-scale responses, an RCM is forced with large-scale weather analyses at the boundaries in a typical simulation. Unlike the conventional approach, forcing in SN is conducted not only at the lateral boundaries but also in the interior. This interior forcing is maintained by adding nudging terms in the spectral domain, with maximum efficiency for large scales and no effect for small scales. The SN technique was first applied to WRF, version 3.1, by Miguez-Macho et al. (2004, 2005). In the SN for WRF, a new term is added to the tendencies of the variables that relax the selected part of the spectrum to the corresponding waves from the reanalysis:

$$\frac{dQ}{dt} = L(Q) - \sum_{|n|\le N} \sum_{|m|\le M} K(Q_{mn} - Q_{d_{mn}}) e^{ik_m x} e^{ik_n y}, \tag{1}$$

where Q is any of the prognostic variables to be nudged, L is the model operator, and Q_d is the variable from the driving fields; Q_{mn} and $Q_{d_{mn}}$ are the spectral coefficients (also named expansion coefficients in the Fourier expansion technique) of Q and Q_d, respectively, which are calculated by decomposing the difference fields $Q - Q_d$ in Fourier series; and K is the nudging coefficient, which denotes the strength of the SN technique (s^{-1}); in addition, m and n are the wavenumbers in the zonal and meridional directions in the Lambert projection, which roughly correspond to the east–west and north–south directions, respectively. The wave vector components k_m and k_n in the zonal and meridional directions depend on the domain sizes D_x and D_y in the corresponding direction and wavenumbers, as follows:

$$k_m = \frac{2\pi m}{D_x}; \quad k_n = \frac{2\pi n}{D_y}. \tag{2}$$

The variables nudged in this study are horizontal winds, temperature, and geopotential height. We chose not to nudge moisture fields, because their variations in the horizontal, and especially in the vertical, can be very pronounced and are likely to be missed by coarse-resolution reanalysis (Miguez-Macho et al. 2004, 2005). The variables in the PBL were not nudged because of the strong coupling of the atmosphere and land surface there; thus, the atmospheric state at lower levels was free to adjust to surface properties and forcings (Miguez-Macho et al. 2004, 2005; Lo et al. 2008). In the SN techniques available in the public releases of WRF,

TABLE 1. Summary of experimental design.

Expt No.	Expt Name	Wavenumber*	Nudging height	Nudging period
1	NoNU	None	None	None
2	w2_850_short	$m = n = 2$	Above 850 hPa	24 h
3	w3_850_short	$m = n = 3$	Above 850 hPa	24 h
4	w6_850_short	$m = n = 6$	Above 850 hPa	24 h
5	w2_850_whole	$m = n = 2$	Above 850 hPa	31 days
6	w3_850_whole	$m = n = 3$	Above 850 hPa	31 days
7	w6_850_whole	$m = n = 6$	Above 850 hPa	31 days
8	w3_700_whole	$m = n = 3$	Above 700 hPa	31 days
9	w3_500_whole	$m = n = 3$	Above 500 hPa	31 days

* In this column, m and n refer to wavenumbers in the zonal and meridional directions, respectively.

the nudging coefficient K is a constant set by WRF users. In contrast, in the method of Miguez-Macho et al. (2004, 2005), K is zero in the boundary layer and increases smoothly from about 1500 m above the terrain to become constant in the upper troposphere. However, WRF users can set the height (the model layer) above which the SN is turned on.

c. Experiments with spectral nudging

Nine experiments were conducted in this study to investigate the effects on performance in projecting near-surface fields when SN was applied to different wavenumbers, nudging durations, and altitudes. The first experiment was the control experiment (NoNU), a 1-month run without the nudging technique. For the second, third, and fourth experiments, SN was turned on above 850 hPa, and different wavenumbers were assigned (Table 1) during the spinup period, which has benefits of smoothing the start of analysis periods and avoiding possible false sources and sinks (Dudhia 2012). To evaluate the impacts of nudging duration on the performance of SN in dynamical downscaling, the time period with nudging application was extended to the entire integrated period (see Table 1) in the fifth, sixth, and seventh experiments, with different wavenumbers for comparison with calculations using nudging during the spinup period only. For the eighth and ninth experiments, the nudging was applied at higher altitudes (see Table 1) to 700 and 500 hPa to investigate the variations in SN performance in near-surface fields. The nudging coefficients for all variables were set at $0.0003\ s^{-1}$. During the simulation, nudging was conducted every 6 h, consistent with the frequency of the R-2 data. All experiments employed the same model domain, relaxation zones, physics options, initial conditions, and boundary conditions, and the simulation periods were identical to that of the control experiment. In section 3, we use the experiment numbers shown in Table 1 to represent different nudging experiments.

3. Results

For a better evaluation of model performance, we divided the portion of the CONUS without oceans and lakes (30°–49°N, 122.5°–81°W) into four subregions according to differences in topography (as show in Fig. 1) and climatological characteristics (Mearns et al. 2012). These four regions are termed the northwest region (NWR; 40°–49°N, 122.5°–106°W), the northeast region (NER; 40°–49°N, 106°–87.5°W), the southwest region (SWR; 32.5°–40°N, 120°–102°W), and the south-central region (SCR; 30°–40°N, 102°–81°W). In the following sections, we evaluate the performance of simulations at these selected regional scales. The closed triangles and the short names in the following figures will be used to evaluate the performance of simulation in observed fields over weather stations strategically located around the CONUS and near large defense installations, a focus of our ongoing downscaling study.

a. Control simulation

Figure 2 shows the NARR data and NRCM-simulated monthly accumulated precipitation, monthly average surface temperature, and 10-m wind speed and direction without nudging over the CONUS. The NRCM simulation (Fig. 2b) basically reproduces the spatial pattern of precipitation shown in Fig. 2a (NARR data), with additional precipitation over SCR and NER and less precipitation over NWR and SWR. However, NRCM overestimated the precipitation over the bottom-right corner of SCR, while it underestimated the precipitation over the other parts of SCR and the bottom part of NER. We have provided a corresponding set of figures in the appendix using an absolute scale for easier interpretation. For example, Fig. A1a is the same as Fig. 2a. The NRCM simulation (Fig. 2d) also captured the spatial pattern of surface temperature well (Fig. 2c), with lower temperatures over NWR and NER and higher temperatures over SWR and SCR. Nevertheless, the model underestimated the surface temperature by about 2°–5°C or more over almost all of the CONUS, especially over NWR, NER, and SCR. An evaluation of the performance of NRCM for 2-m temperature (data not shown) showed a feature similar to that in surface temperature, 1°–3°C lower than NARR data over all of CONUS, although the NARR 2-m temperature dataset is 1°C higher than the observations (Mesinger et al. 2006). The performance of NRCM for 10-m wind speed and direction (Fig. 2f) compares unfavorably to the NARR data (Fig. 2e). For example, the high southerly

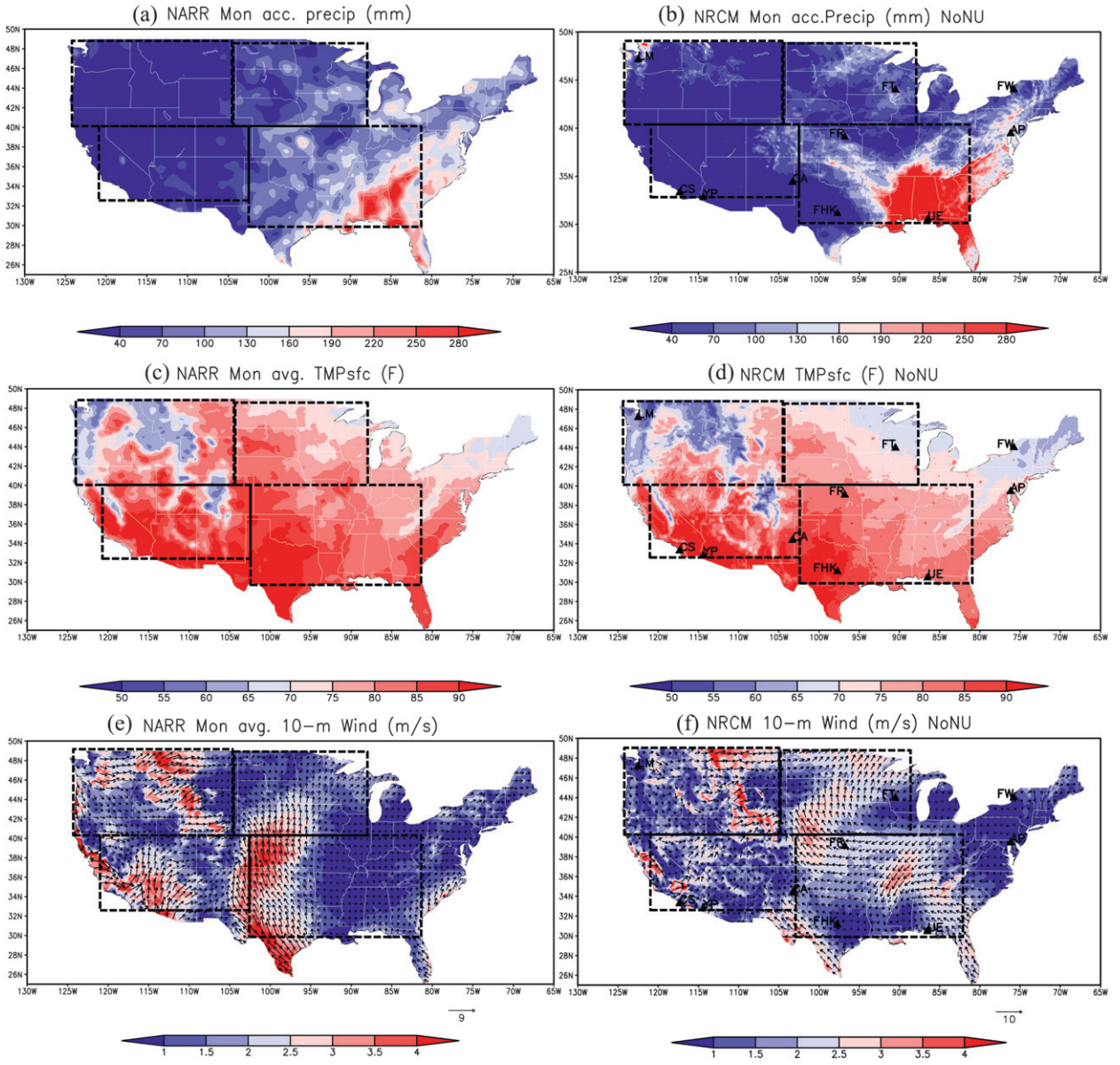

FIG. 2. Comparison of (a),(b) monthly accumulated precipitation (mm month^{-1}), (c),(d) monthly averaged surface temperature (°F), and (e),(f) 10-m wind (m s^{-1}) for (left) NARR and (right) NRCM simulation with no nudging for July 2005. Four distinct regions are labeled: NWR (40°–49°N, 122.5°–106°W), NER (40°–49°N, 106°–87.5°W), SWR (32.5°–40°N, 120°–102°W), and SCR (30°–40°N, 102°–81°W).

wind flow (Fig. 2e) over the left part of SCR drifts toward the right part of SCR with northerly wind, and the wind speed over the upper part of NER is also much higher than the NARR data.

b. Sensitivity to wavenumbers in SN

To improve model performance in near-surface fields, different SN choices were applied. Here, we describe the sensitivities of the model to different choices of SN. The choice of wavenumbers is determined by the size of the modeling domain and the scale of the driving forces that the RCM should retain (Liu et al. 2012). If the wavenumber is too large, then the results of SN would be similar to those of grid nudging, because the nudged scale is too small. If the wavenumber is too small, then the nudging technique cannot represent enough energy to force the RCMs. Liu et al. (2012) suggested wavelengths of about 2000 km to predict precipitation, temperature, and horizontal kinetic energy, and Cha et al. (2011) applied SN with wavelengths of about 1000 km

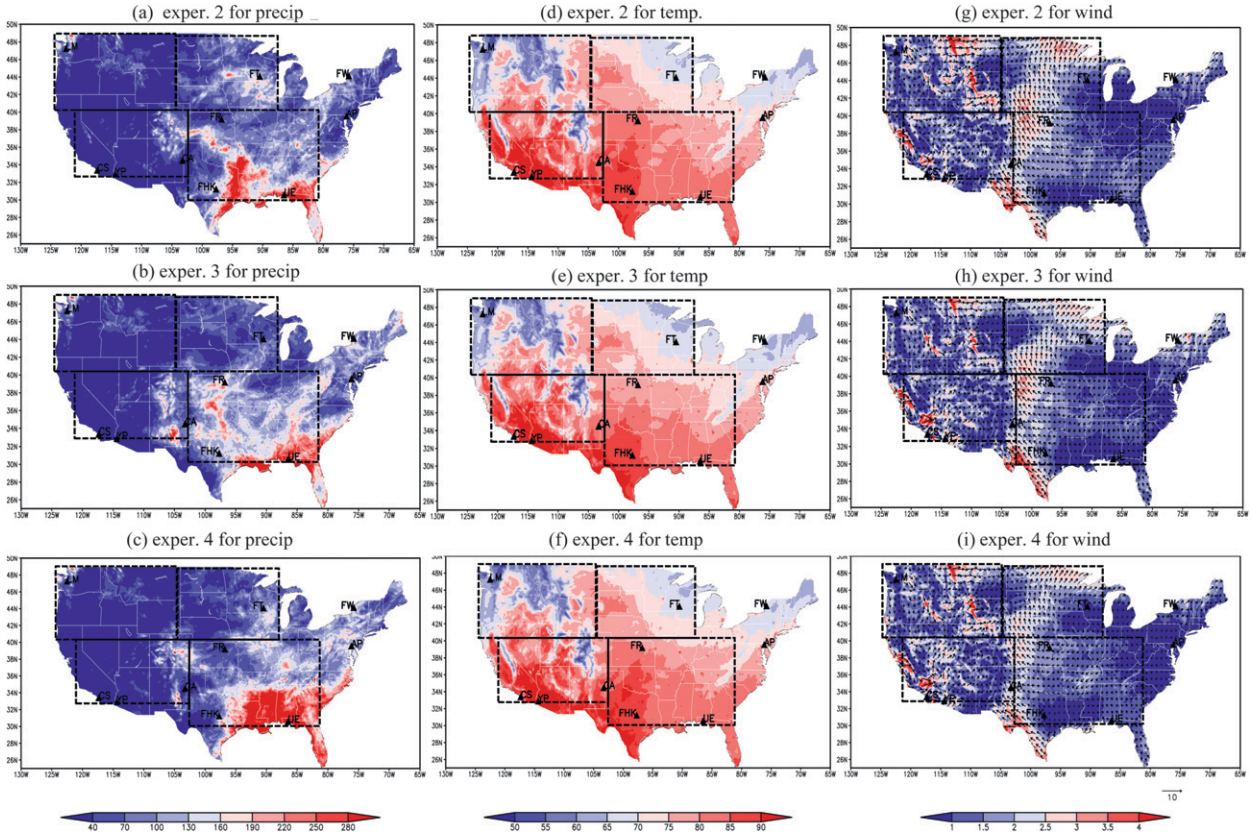

FIG. 3. Comparison of (a)–(c) monthly accumulated precipitation, (d)–(f) monthly averaged surface temperature, and (g)–(i) 10-m wind speed and direction for spectral nudging techniques with wavenumbers (top) 2, (middle) 3, and (bottom) 6 during short nudging periods. The nudging techniques were conducted for 24 h.

to forecast the wind component. In this study, we employed wavenumbers of 2, 3, and 6 in both zonal and meridional directions, yielding wavelengths of about 3000, 2000, and 1000 km for the evaluation of the performance of SN in near-surface fields.

Figures 3a–c show monthly accumulated precipitation nudged by two, three, and six waves, respectively, for 24 h. Experiments 2 and 3 (Figs. 3a,b) resulted in significantly depressed precipitation over the bottom-right corner of SCR, which more closely resembles NARR data than NoNU. However, experiment 2 calculated spurious rainfall area over the bottom-right part of SCR, and experiment 4 calculated a broader rainfall area than the NARR data show. Another positive effect of experiment 3 is the significant increase in precipitation over the other parts of SCR relative to NoNU. All three experiments slightly increased the precipitation over the lower parts of NER, more like the distribution of the NARR data, but all three experiments generated more rainfall over SWR than the NARR data show.

Figures 3d–f show the monthly average surface temperature nudged by the same approaches as for precipitation. The results show no significant improvement for the three SN approaches over NoNU, and the nudged surface temperatures over NER and SCR are even lower than the NARR data. Moreover, for surface temperature the performance of experiment 3 is slightly worse than that of the other two experiments, since the differences between experiment 3 and NARR are slightly larger than the other two (see the appendix). Also, the effects of wavenumbers on 2-m temperature (data not shown) showed features like those for surface temperature. The reason for no improvement in temperature by SN is possibly the short nudging duration; the RCM simulates the temperature primarily on the basis of local driving forces and becomes independent of nudging quickly.

Figures 3g–i show the monthly average 10-m wind speed and direction by the same nudging approaches used for precipitation and surface temperature. The results show significant improvements in wind speed and direction over SCR for all three experiments and slight improvements over NER for both experiments 3 and 4. The high wind speed and north wind over the right part of SCR have been moved back to the left part, which is

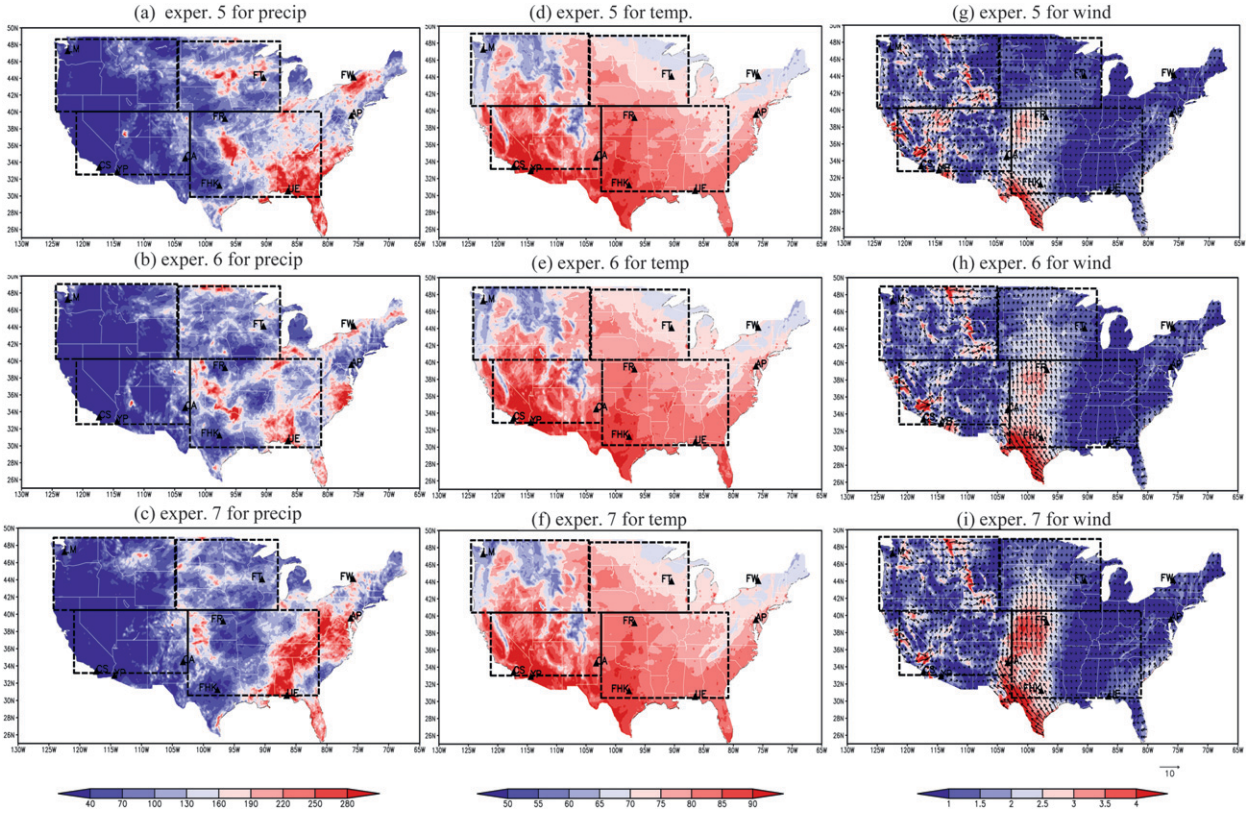

FIG. 4. As in Fig. 3, but with nudging techniques conducted for 31 days.

closer to the NARR data than to NoNU. However, significant differences remain in the calculated wind fields over the central SCR and the top part of NER compared to the NARR data.

c. *Sensitivity to nudging duration periods in SN*

To evaluate nudging duration, we extended the nudging periods and conducted the nudging techniques during the entire period of integration (31 days) with two, three, and six waves, respectively, to investigate how well the nudging techniques performed in downscaling near-surface fields. Figures 4a–c show the monthly accumulated precipitation nudged by two (experiment 5), three (experiment 6), or six (experiment 7) waves during the entire integration period. In comparison with Fig. 3, the whole-period nudging techniques produced much more rainfall over most parts of the four subregions than the NARR data show. However, rainfall over SCR showed slight improvement, especially for experiment 7, which performed better not only in rainfall amount but also in spatial distributions than did experiment 4 (conducted with the same wavenumber but a different nudging duration).

Figures 4d–f show the surface temperature nudged by the techniques used for precipitation. The results show increments of 5°–10°F in surface temperature versus NoNU (Fig. 2d) and the experiments with short nudging duration (Figs. 3d–f), especially over NWR, NER, and SWR. This observation indicates that the whole-period nudging techniques represent a significant improvement in simulating surface temperature. The temperatures for experiments 6 and 7 are closer to NARR data (Fig. 2c) than are the experiment 5 results over NER, since the differences between experiment 6 (and 7) and NARR are 0°–4°C smaller than that between experiment 5 and NARR over NER, while the temperatures for experiments 5 and 7 are closer to the NARR data than are the experiment 6 results over NWR. The 2-m temperature nudged in experiment 7 (data not shown) indicated identical improvements over NWR and NER.

The superiority of the whole-period nudging techniques becomes more apparent in comparisons of the 10-m wind (Figs. 4g–i) with NARR data (Fig. 2e) and the short-term nudging results discussed in section 3b (Figs. 3g–i). The high wind speed area over the right part of SCR has completely moved to the left part, and the high wind speed area over the top part of NER is significantly decreased, both much closer to the NARR data. In particular, of the three experiments, experiment 7

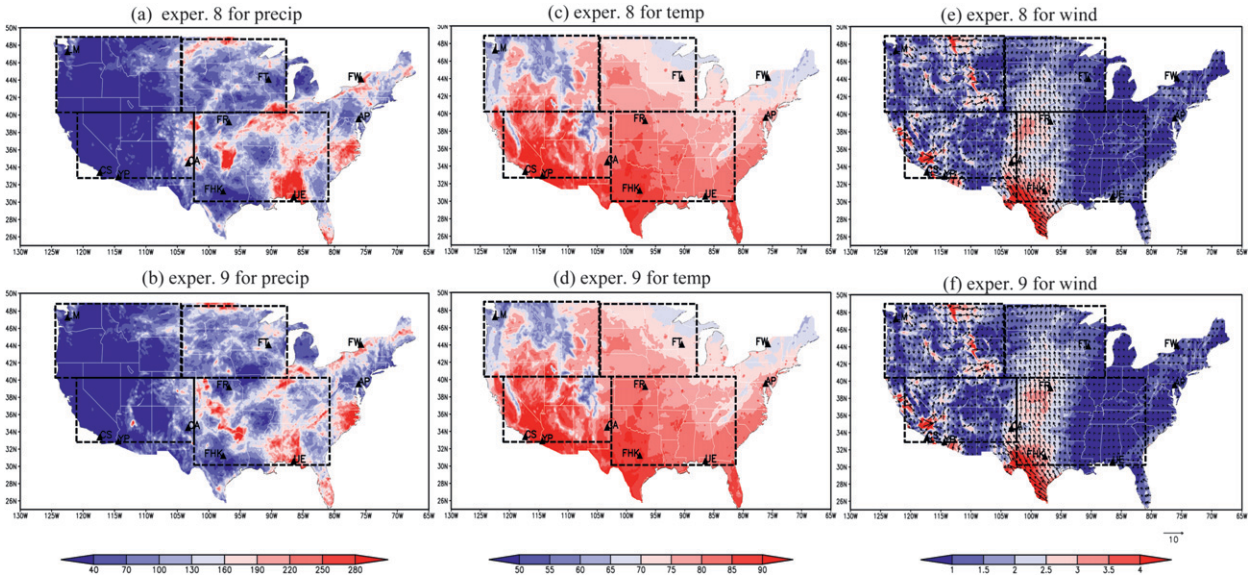

FIG. 5. Comparison of (a),(b) monthly accumulated precipitation, (c),(d) monthly averaged surface temperature, and (e),(f) 10-m wind for spectral nudging techniques above (top) 700 and (bottom) 500 hPa with wavenumber = 3 during the nudging period of 31 days.

performed the best in wind direction and speed over SCR and NER, which most resemble the NARR data shown in Fig. 2e. The wind speed over the left-middle part of SCR in experiments 5 and 6 and that over NER in experiment 5 are much slower than the NARR data. All of the nudging techniques, including short-period and whole-period nudging, presented much slower wind speeds when forecasting the wind fields over the western part of the CONUS, especially over the bottom-left part of SWR and the top-right part of NWR.

d. Sensitivity to height of application of SN

The topography over the CONUS is varied and complex, with high mountains through the southwest to the northwest accounting for approximately half of the CONUS area. Consequently, the nudging height could affect model performance in near-surface fields. If the nudging height was too low, then the model surface variables, which have short time scales and large wavenumbers, would be adjusted often and produce noisy results. Therefore, we designed two experiments with the nudging heights elevated to 700 and 500 hPa to test the sensitivities of model performance to nudging heights. Because the performance of different SN techniques varied over the four subregions, here we only applied nudging techniques with three waves during the entire period of model integration. Figure 5 shows the simulated precipitation (Figs. 5a,b), surface temperature (Figs. 5c,d), and 10-m wind (Figs. 5e,f) with nudging application above 700 and 500 hPa. The results show no significant difference in precipitation, temperature, and wind when SN was applied above 850 hPa (experiment 6; Figs. 4b,e,h) or above 500 hPa (experiment 9; Figs. 5b,d,f). However, the results show much more rainfall over SCR (Fig. 5a), slightly lower surface temperature over some parts of NER and SCR (Fig. 5c), and slower 10-m wind speeds (Fig. 5e) over SCR in experiment 8 than in experiments 6 and 9. These results do not agree well with the NARR data.

e. Evaluation statistics and ranks

To further evaluate and compare the performance of different SN techniques in near-surface fields, we performed statistical analyses by comparing the SN grid values with NARR grid data over distinct subregions. To facilitate comparisons, we interpolated the 32-km NARR data onto the 12-km WRF grid with the inverse-distance-squared weighting method. We also applied two different statistical approaches. One is the root-mean-square error (RMSE; Lo et al. 2008; Mearns et al. 2012), which provides information on model performance at the subregional scale. Small values of RMSE indicate slight disagreements in subregional average precipitation (or temperature, or wind) between the simulation and the NARR data. The other statistical approach is the pattern correlation coefficient (COR; Giorgi et al. 2012; Mearns et al. 2012), which indicates the strength and direction of a spatial relationship between the simulation and NARR data. Large values of COR mean that the spatial distribution of simulated precipitation (or temperature, or wind) agrees well with the NARR data. Inconsistencies between these two

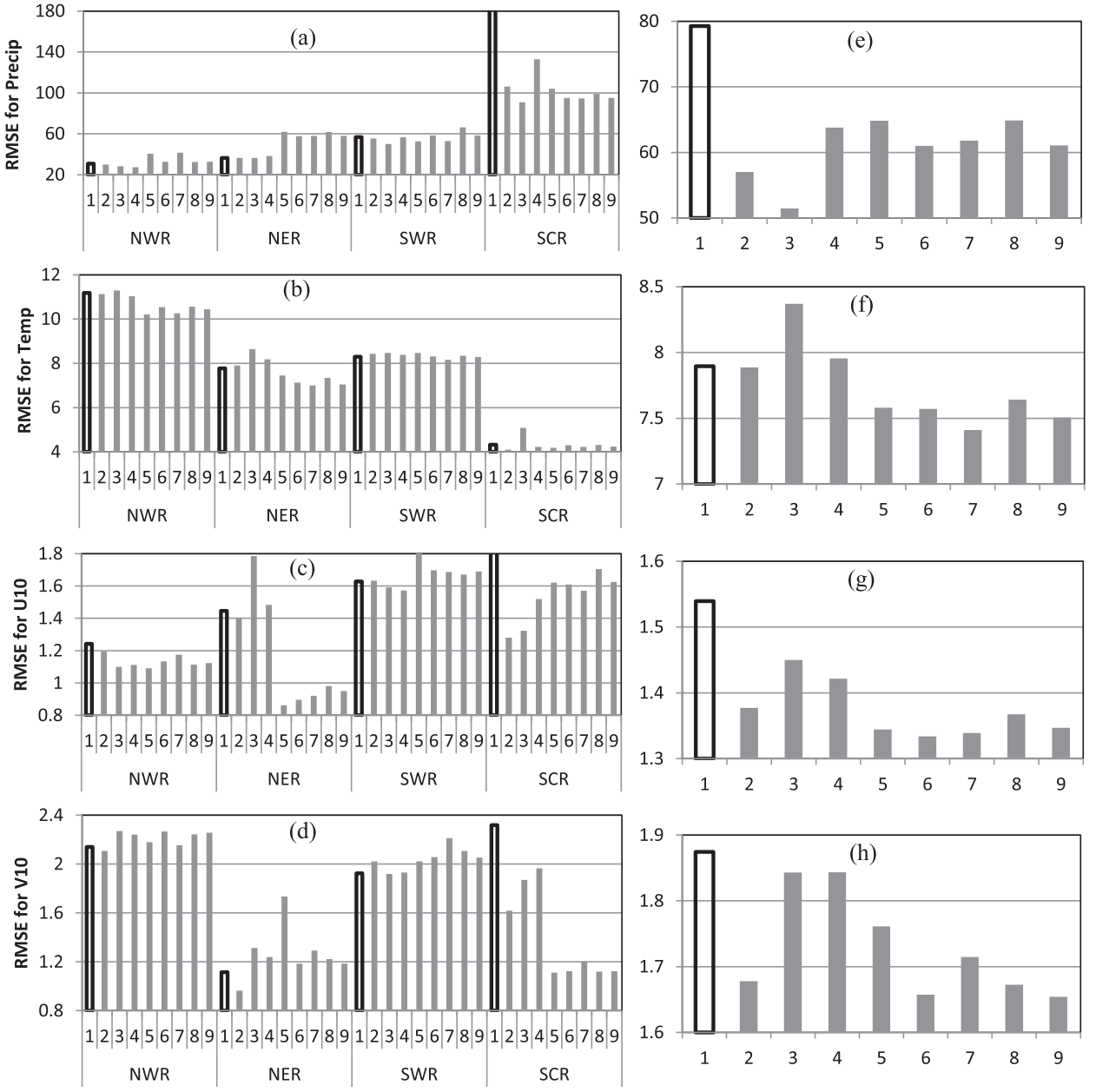

FIG. 6. RMSEs for NoNU and nudging experiments for July 2005 over the four subregions: (a) precipitation (mm month^{-1}), (b) surface temperature (°C), (c) 10-m zonal wind, and (d) 10-m meridional wind (m s^{-1}). (e)–(h) As in (a)–(d), but showing the averages of the four subregions. The numbers on the horizontal axis are the experiment numbers shown in Table 1.

verification approaches are possible; for example, RMSE could be small because of the slight differences between the simulated and observed subregional average precipitation (or temperature, or wind), while COR could be small because of the poor agreement of the simulation with the observed spatial pattern of precipitation (or temperature, or wind). Therefore, applying the two statistical approaches together improves the evaluation of model performance.

Figure 6a shows the evolution of RMSE for the simulated monthly accumulated precipitation over the four distinct subregions. In comparison with NoNU (experiment 1), SN significantly decreased RMSE values for simulated precipitation over SCR, although these RMSE values exceed those of the other three subregions, implying that SCR is a sensitive, optimal region for testing the performance of SN for precipitation. The RMSE values were much smaller in the short-period nudging

experiments (experiments 2, 3, and 4) than in the whole-period nudging experiments (experiments 5, 6, and 7) over NWR and NER, and the RMSE values generated by experiment 3 were close to the minimum for all nudging experiments over the four subregions, implying that experiment 3 is the best SN technique for improving the performance of NRCM in simulating precipitation over all subregions. The RMSE values for the three experiments with nudging applications above different altitudes (experiments 6, 8, and 9) were not significantly different. Among these, experiments 6 and 9 presented slightly smaller RMSE values than did experiment 8 over NER, SWR, and SCR.

Figure 6b shows the evolution of RMSE of the simulated monthly average surface temperature over the four distinct subregions. In general, the SN techniques generated the smallest RMSE values over SCR and the largest values over NWR. The short-period nudging techniques (experiments 2–4) did not substantially decrease the RMSE values, and experiment 3 even increased the RMSE values over NER and SCR. All of the whole-period nudging experiments presented smaller RMSE values than did short-period nudging over the four subregions, except that the nudging techniques resulted in no significant improvement over SWR. RMSE values for the SN techniques applied above different heights were not significantly different, except that experiment 8 generated slightly larger RMSE values than did experiments 6 and 9.

Figures 6c and 6d show the evolution of the RMSE of the simulated monthly average zonal wind (U10) and meridional wind (V10) over the four distinct subregions. In general, the errors of the model occurred mainly over the western CONUS, with larger RMSE values for V10 over NWR and SWR and for U10 over SWR than over NER and SCR. In fact, the SN techniques generated even larger errors than did NoNU. Significant differences between various nudging techniques were observed over NER and SCR: the short-period nudging techniques presented larger RMSE values for U10 over NER and for V10 over SCR than the whole-period nudging techniques, which are closer to the NARR data. RMSE values between the SN techniques applied above at different altitudes (experiments 6, 8, 9) were not significantly different, except that the performance of experiment 8 was slightly inferior for zonal wind over NER and SCR.

Figures 6e–h show the four-subregion-average RMSE values for precipitation, surface temperature, and 10-m wind in the nine experiments. Experiment 3 shows the smallest RMSE value for precipitation (Fig. 6e), while experiment 7 shows the smallest RMSE value for surface temperature (Fig. 6f), and most of the whole-period nudging techniques show smaller RMSE values than the short-period nudging techniques for 10-m zonal and meridional winds (Figs. 6g,h). To further verify the results shown above, we interpolated NRCM precipitation, surface temperature, and wind components to the resolution of NARR (32 km) using the same method as mentioned above. Results showed that, although this interpolation subtly increased RMSE values of all the concerned variables in this study, the differences in RMSE values over distinct regions and for the nine model simulations were similar to the interpolation from NARR (32 km) to NRCM (12 km). Because the COR value reflects a spatial relationship between simulation and observation, here we show the COR values obtained for different nudging experiments and NARR data over the entire portion of the CONUS (30°–49°N, 122.5°–81°W) that includes the four subregions. All of the COR values in Fig. 7 pass the confidence test with a significance level of 0.02. All of the SN techniques significantly improved the COR values for precipitation (Fig. 7a) versus NoNU, with a COR value larger than 0.37. The largest COR value (larger than 0.5) for experiment 3 indicates that the spatial distribution of nudged precipitation agrees quite well with the NARR data. This agreement is also indicated by RMSE values (Fig. 6e).

Figure 7b shows the evolution of COR for surface temperature over the entire portion of the CONUS. The COR values generated by short-period nudging were smaller than for NoNU, while the values generated by the whole-period nudging were much larger than for NoNU. These results indicate that the whole-period SN techniques significantly strengthened the relationship of the spatial patterns of simulated and NARR temperatures, in agreement with the results of the RMSE analysis.

Figures 7c and 7d illustrate the evolution of COR for 10-m zonal and meridional wind fields over the entire portion of the CONUS. All of the SN techniques enhanced the COR values in comparison with NoNU, except that experiment 5 for V10 had a slightly smaller COR value than did NoNU. Experiment 2 had the largest COR value for U10 and V10, mainly because the nudged wind directions agreed well with the NARR data, according to our further explorations. The performance of SN applied above 700 hPa was slightly inferior to the performance above 850 and 500 hPa, a result also reflected by RMSE values in Figs. 6g and 6h.

To select an optimal SN technique for application in NRCM to forecast the near-surface fields, we comprehensively considered the performance of each SN technique in precipitation, surface temperature, and 10-m wind field over the four subregions and ranked all the SN techniques according to RMSE and COR values (Table 2). To generate a composite index and eliminate

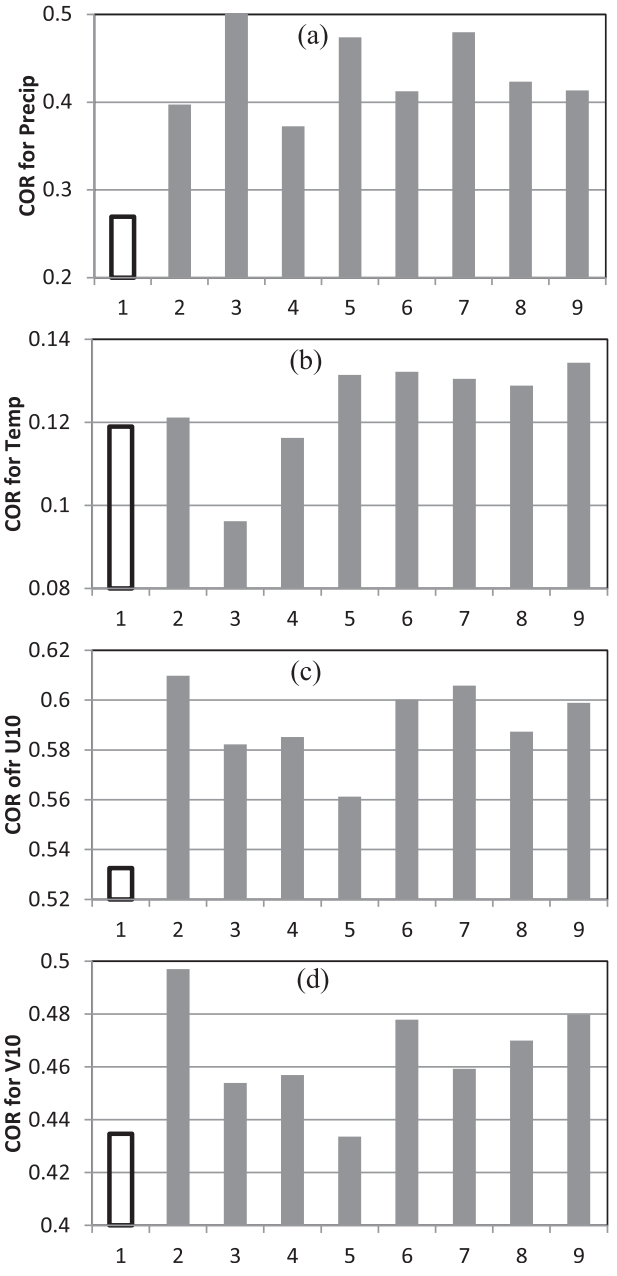

FIG. 7. Pattern correlation coefficient for NoNU and nudging experiments for July 2005 over the entire portion of the CONUS (122.5°–81°W, 30°–49°N): (a) precipitation, (b) surface temperature, (c) 10-m zonal wind, and (d) 10-m meridional wind. The numbers on the horizontal axis are the experiment numbers shown in Table 1.

the differences in RMSE values for different surface fields, we first set up an ensemble of scores from 100 to 0 with two scores decreasing, resulting in 50 bins in this ensemble of scores. Accordingly, we divided all of the RMSE values for precipitation (or temperature, or wind) for different SN techniques into 50 bins and gave each SN technique a score. We then replaced the RMSE values with scores from 100 to 0 for the different surface fields and calculated the composite score (Table 2, left side) by giving one-third to precipitation, one-third to temperature, one-sixth to the zonal wind field, and one-sixth to the meridional wind fields. We also calculated composite COR values (Table 2, right side) for the different SN techniques with the same ratios for precipitation, temperature, and wind as for the composite scores. Table 2 shows that all of the SN techniques performed better than NoNU. Experiment 7 showed the most significant improvement of all the SN techniques, decreasing the errors and improving the spatial pattern of NRCM by more than 30.5% versus NoNU. The performance of experiment 4 was poorest in improving the accuracy and spatial distribution of NRCM, with only a 15.7% improvement versus NoNU. We also conducted a *t* test on the differences between the NoNU and SN experiments, and the results show that these improvements in the SN experiments were mainly contributed by the simulated precipitation over the entire CONUS and wind components over the eastern CONUS, while the improvements in simulated temperature are not significant.

TABLE 2. Ranked performance of the different SN techniques, according to the results of statistical verification. The optimal SN technique is in boldface type.

Composite RMSE score			Composite COR value		
Expt			Expt		
No.	Name	Score	No.	Name	COR
7	**w6_850_whole**	**58.08**	**7**	**w6_850_whole**	**0.381**
6	w3_850_whole	57.25	3	w3_850_short	0.374
9	w3_500_whole	57.25	5	w2_850_whole	0.368
2	w2_850_short	56.75	9	w3_500_whole	0.362
8	w3_700_whole	55.67	6	w3_850_whole	0.361
5	w2_850_whole	55.17	8	w3_700_whole	0.360
3	w3_850_short	53.08	2	w2_850_short	0.357
4	w6_850_short	51.50	4	w6_850_short	0.337
1	NoNU	44.50	1	NoNU	0.291

4. Summary and discussion

a. Summary

The performance of eight SN techniques—with different wavenumbers and nudging duration periods above different layers of the model—was examined for application in the downscaling of R-2 data with the NRCM. Near-surface fields including precipitation, surface temperature, 2-m temperature, and 10-m wind were evaluated against another set of high-resolution reanalysis data (NARR). Our evaluation focused on four subregions of the CONUS during July 2005, and we employed two

statistical approaches, RMSE and COR, over the subregions.

We demonstrated significant differences between the eight SN experiments. The RMSE and COR values showed that experiment 3 is the best SN technique for forecasting precipitation, while the whole-period nudging techniques performed better than the short-period nudging for forecasting the surface and 2-m temperature and 10-m wind, except that experiment 2 showed a higher COR value for 10-m wind. In addition, the performance of different SN techniques varied substantially over the four subregions, which indirectly proves that our regional subdivision was reasonable and helpful in evaluating and comparing the performance of diverse SN techniques. Nevertheless, we found no significant differences among SN techniques applied above 850, 700, and 500 hPa, except that the performance of the nudging technique applied above 700 hPa was slightly inferior to that above the other two altitudes.

As a basis for improving forecasts in the near-surface fields with SN techniques, we ranked the performances of our eight SN techniques according to two different composite indexes: RMSE scores and COR values. The results showed that experiment 7 (wavenumber 6, nudging above 850 hPa for 31 days) is the optimal SN technique for predicting near-surface fields over the entire region (30°–49°N, 122.5°–81°W) of the CONUS studied. This combination not only generated the smallest errors for the NRCM model (RMSE score) but also showed the strongest spatial relationship with the NARR dataset (COR value).

b. Discussion

In section 3e, statistical metrics were calculated for each of the four subregional comparisons indicated in Figs. 2–4, as well as with respect to the NARR dataset, both because it is available for the domain and because its resolution best matches the model resolution. We recognize that different datasets and different regional divisions can cause significant differences, and therefore the statistical values should be considered only as indicative rather than certain. It should be noted that, although there are significant differences in precipitation between NARR and TRMM 3B42 over California, the precipitation here is often very light. For example, the observed (TRMM) monthly accumulated precipitation is less than 30 mm for July 2005, and the daily mean precipitation is less than 1 mm for 1998–2010 in the study of Pu et al. (2012). Therefore, we believe that NARR precipitation can be viewed as a reasonable criterion for verifying the NRCM precipitation in our study.

Most of the precipitation in summer is associated with convection. Therefore, if the Grell–Devenyi convective parameterization (Grell et al. 1994) produced too few or too many cumulus clouds, the result would be an under- or overestimation of precipitation and a relatively high RMSE and low COR. This issue is another uncertainty or a key source for errors that should be considered when model performance over different subregions is evaluated. For example, the poorest performance of the model in precipitation over SCR, as shown by RMSE and COR values, was most likely induced by the incomplete cumulus parameterization; however, precipitation over the western regions with high mountains could be influenced more by topography than by model physics (Caldwell et al. 2009), resulting in smaller RMSE and larger COR values than over SCR.

From the differences between simulated surface temperature and NARR data (Figs. A1–A4), we found that the simulated temperature is more than 5°C higher than the NARR data over California and southwest Texas. Caldwell et al. (2009) suggested that the warm bias pattern of temperature over California is consistent with low summertime soil moisture. By comparing the simulated four-layer soil moisture with the NARR data, we also found that the simulated soil moisture is lower than the NARR data over most of the CONUS; this should induce a warmer temperature pattern over most of the CONUS area. However, in this study, the simulated surface temperature (including NoNU and nudging) was 2°–6°C (even more) lower than the NARR data over most of the CONUS area. One of the most important possible reasons for the low temperature is that the land-use data employed in this study, supplied by the U.S. Geological Survey for 1992–93, could not completely represent the land-use and land-cover changes because of anthropogenic influences that have induced significant surface warming during the past dozen years (Pielke et al. 2002; Kalnay and Cai 2003). Therefore, the land-use and land-cover data should be modified to describe the modern land surface features and improve the calculation of surface temperature (Sertel et al. 2010; Trusilova et al. 2008). In addition, the largest biases in surface temperature over NWR with high mountains suggest that topographic elevation and slope aspect might also be responsible for uncertainty in the model (Caldwell et al. 2009).

Acknowledgments. We thank two anonymous reviewers for their constructive comments. This work was supported under a military interdepartmental purchase request from the SERDP, RC-2242, through U.S. Department of Energy Contract DE-AC02-06CH11357.

APPENDIX

Corresponding Set of Figures

Figures A1–A4 correspond to the figures used in the text, but with absolute scales.

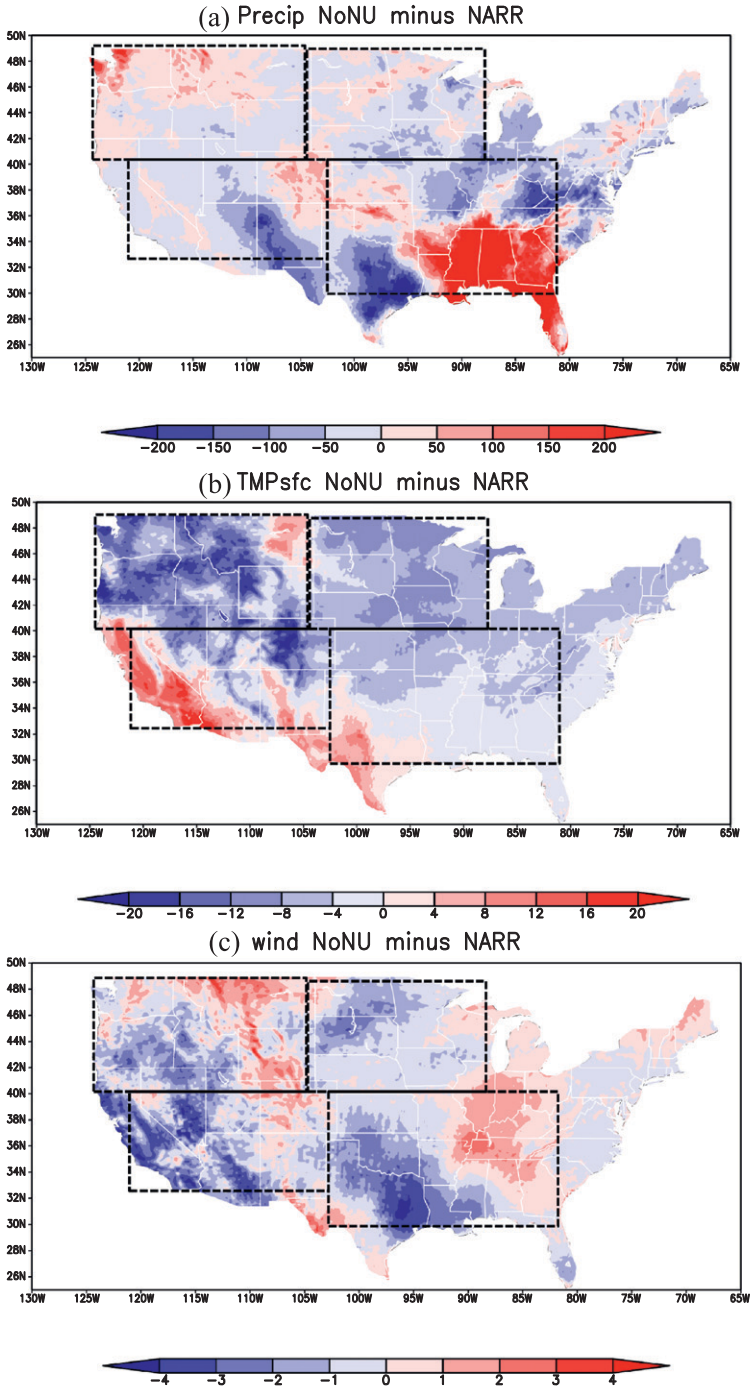

FIG. A1. Differences in (a) monthly accumulated precipitation (mm month^{-1}), (b) monthly averaged surface temperature (°C), and (c) 10-m wind speed (m s^{-1}) between NARR and NoNU for July 2005.

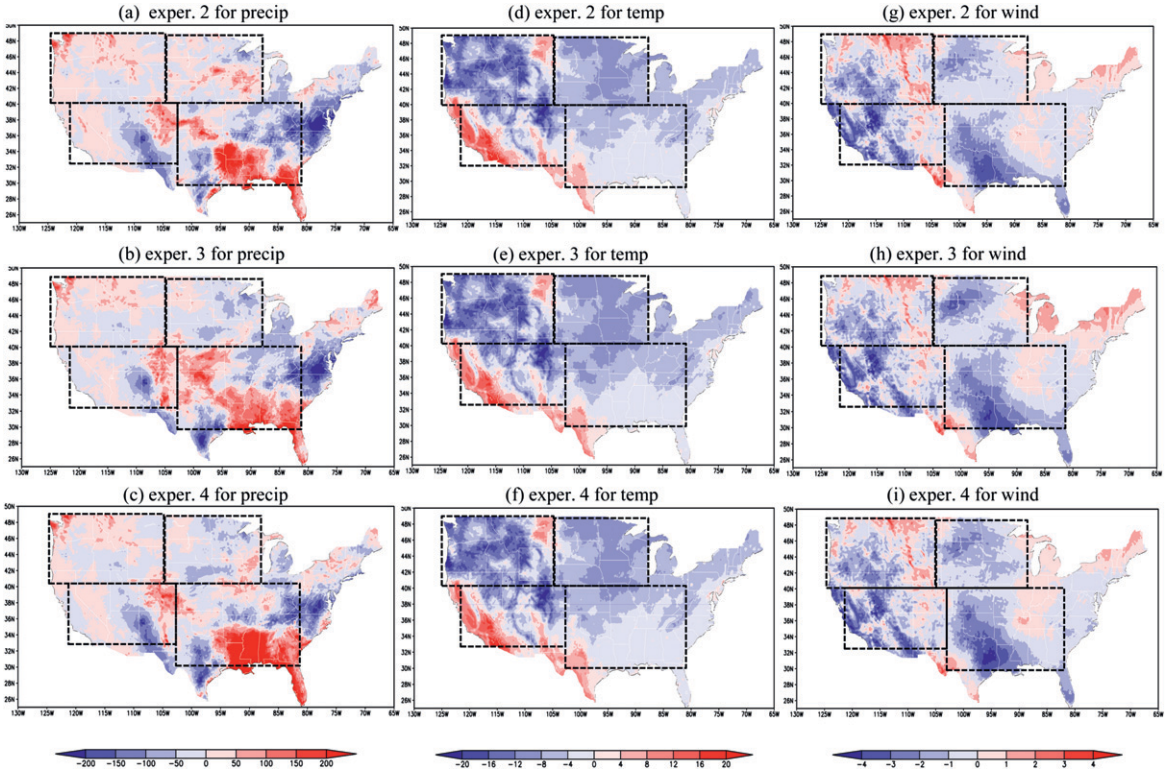

FIG. A2. As in Fig. A1, but between NARR and SN experiments 2–4.

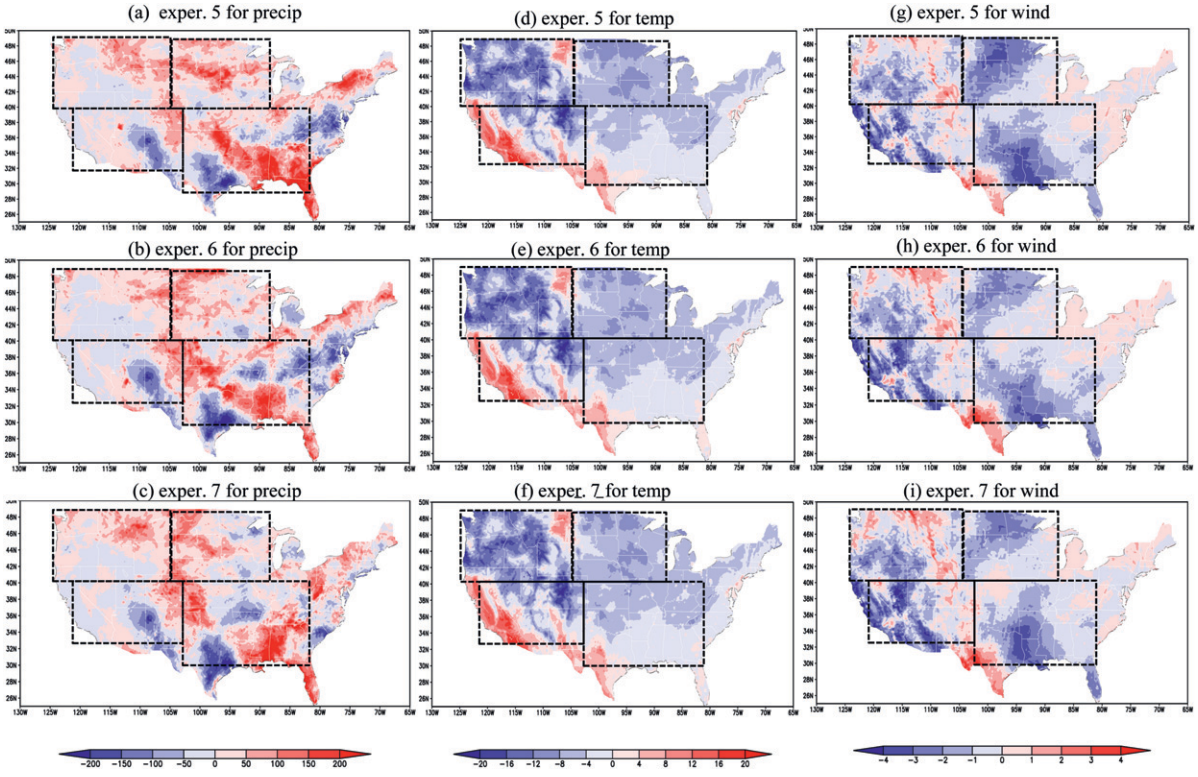

FIG. A3. As in Fig. A1, but between NARR and SN experiments 5–7.

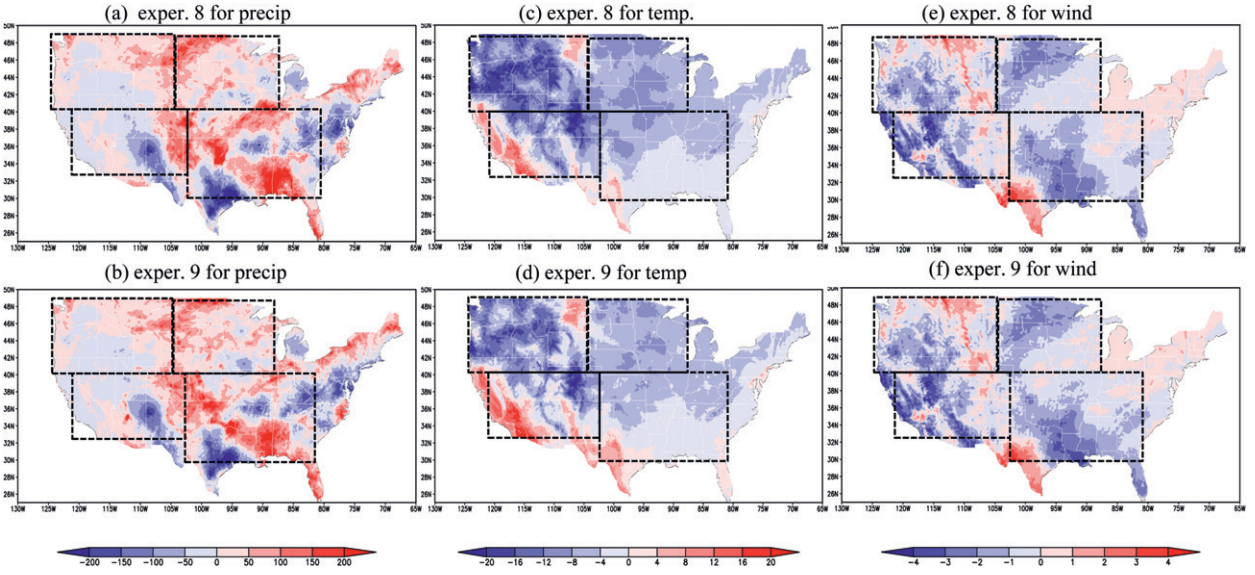

FIG. A4. As in Fig. A1, but between NARR and SN experiments 8 and 9.

REFERENCES

Caldwell, P., H. S. Chin, D. C. Bader, and G. Bala, 2009: Evaluation of a WRF dynamical downscaling simulation over California. *Climatic Change,* **95,** 499–521.

Carter, T. R., M. L. Parry, H. Harasawa, and S. Nishioka, 1994: IPCC technical guidelines for assessing climate change impacts and adaptions. Cambridge University Press, 59 pp.

Cha, D. H., C. S. Jin, D. K. Lee, and Y. H. Kuo, 2011: Impact of intermittent spectral nudging on regional climate simulation using Weather Research and Forecasting model. *J. Geophys. Res.,* **116,** D10103, doi:10.1029/2010JD015069.

Chen, F., and J. Dudhia, 2001: Coupling an advanced land surface–hydrology model with the Penn State–NCAR MM5 modeling system. Part I: Model implementation and sensitivity. *Mon. Wea. Rev.,* **129,** 569–585.

Civerolo, K. L., C. Hogrefe, B. Lynn, C. Rosenzweig, R. Goldberg, J. Rosenthal, K. Knowlton, and P. L. Kinney, 2008: Simulated effects of climate change on summertime nitrogen deposition in the eastern US. *Atmos. Environ.,* **42,** 2074–2082.

Davies, H. C., 1976: A lateral boundary formulation for multi-level prediction models. *Quart. J. Roy. Meteor. Soc.,* **102,** 405–418.

——, 1983: Limitations of some common lateral boundary schemes used in regional NWP models. *Mon. Wea. Rev.,* **111,** 1002–1012.

——, and R. E. Turner, 1977: Updating prediction models by dynamical relaxation: An examination of the technique. *Quart. J. Roy. Meteor. Soc.,* **103,** 225–245.

Dudhia, J., 1989: Numerical study of convection observed during the Winter Monsoon Experiment using a mesoscale two-dimensional model. *J. Atmos. Sci.,* **46,** 3077–3107.

——, cited 2012: WRF four-dimensional data assimilation (FDDA). [Available online at http://www.mmm.ucar.edu/wrf/users/tutorial/201001/WRF_FDDA_Dudhia.ppt.pdf.]

Feser, F., 2006: Enhanced detectability of added value in limited-area model results separated into different spatial scales. *Mon. Wea. Rev.,* **134,** 2180–2190.

——, and H. von Storch, 2005: A spatial two-dimensional discrete filter for limited-area-model evaluation purposes. *Mon. Wea. Rev.,* **133,** 1774–1786.

Giorgi, F., 2006: Regional climate modeling: Status and perspectives. *J. Phys. IV France,* **139,** 101–118.

——, and L. O. Mearns, 1999: Introduction to special section: Regional climate modeling revisited. *J. Geophys. Res.,* **104,** 6335–6352, doi:10.1029/98JD02072.

——, M. R. Marinucci, G. T. Bates, and G. D. Canio, 1993: Development of a second-generation Regional Climate Model (RegCM2). Part II: Convective processes and assimilation of lateral boundary conditions. *Mon. Wea. Rev.,* **121,** 2814–2832.

——, and Coauthors, 2012: RegCM4: Model description and preliminary tests over multiple CORDEX domains. *Climate Res.,* **52,** 7–29.

Grell, G. A., J. Dudhia, and D. R. Stauffer, 1994: A description of the fifth-generation Penn State/NCAR Mesoscale Model (MM5). NCAR Tech. Note NCAR/TN-398+STR, 117 pp.

Holland, G. J., J. Done, C. Bruyère, C. Cooper, and A. Suzuki, 2010: Model investigations of the effects of climate variability and change on future Gulf of Mexico tropical cyclone activity. *Proc. 2010 Offshore Technology Conf.,* Houston, TX, Offshore Technology Conference, doi:10.4043/20690-MS.

Hong, S. Y., and J. J. Lim, 2006: The WRF single-moment 6-class microphysics scheme (WSM6). *J. Korean Meteor. Soc.,* **42,** 129–151.

Houghton, J. T., G. J. Jenkins, and J. J. Ephraums, Eds., 1990: *Climate Change: The IPCC Scientific Assessment.* Cambridge University Press, 410 pp.

——, B. A. Callander, and S. K. Varney, Eds., 1992: *Climate Change 1992: The Supplementary Report to the IPCC Scientific Assessment.* Cambridge University Press, 218 pp.

——, L. G. Meira Filho, B. A. Callander, N. Harris, A. Kattenberg, and K. Maskell, Eds., 1996: *Climate Change 1995: The Science of Climate Change.* Cambridge University Press, 572 pp.

Kain, J. S., 2004: The Kain–Fritsch convective parameterization: An update. *J. Appl. Meteor.,* **43,** 170–181.

Kalnay, E., and M. Cai, 2003: Impact of urbanization and land-use change on climate. *Nature,* **423,** 528–531.

Liang, X. Z., K. E. Kunkel, and A. N. Samel, 2001: Development of a regional climate model for U.S. Midwest applications. Part I: Sensitivity to buffer zone treatment. *J. Climate,* **14,** 4363–4378.

Liu, P., A. P. Tsimpidi, Y. Hu, B. Stone, A. G. Russell, and A. Nenes, 2012: Differences between downscaling with spectral and grid nudging using WRF. *Atmos. Chem. Phys.,* **12,** 3601–3610.

Lo, J. C., Z. L. Yang, and R. A. Pielke Sr., 2008: Assessment of three dynamical climate downscaling methods using the Weather Research and Forecasting (WRF) model. *J. Geophys. Res.,* **113,** D09112, doi:10.1029/2007JD009216.

Mabuchi, K., Y. Sato, and H. Kida, 2002: Verification of the climatic features of a regional climate model with BAIM. *J. Meteor. Soc. Japan,* **80,** 621–644.

Mearns, L. O., 2009: Methods of downscaling future climate information and applications National Center for Atmospheric Research. *NARCCAP Users' Meeting,* Boulder, CO, NCAR. [Available online at http://www.narccap.ucar.edu/users/user-meeting-09/talks/Downscaling_summary_for_NARCCAP_Users_Meet09.pdf.]

——, and Coauthors, 2012: The North American Regional Climate Change Assessment program: Overview of phase I results. *Bull. Amer. Meteor. Soc.,* **93,** 1337–1362.

Mesinger, F., and Coauthors, 2006: North American Regional Reanalysis. *Bull. Amer. Meteor. Soc.,* **87,** 343–360.

Miguez-Macho, G., G. L. Stenchikov, and A. Robock, 2004: Spectral nudging to eliminate the effects of domain position and geometry in regional climate model simulations. *J. Geophys. Res.,* **109,** D13104, doi:10.1029/2003JD004495.

——, ——, and ——, 2005: Regional climate simulations over North America: Interaction of local processes with improved large-scale flow. *J. Climate,* **18,** 1227–1246.

Mlawer, E. J., S. J. Taubman, P. D. Brown, M. J. Iacono, and S. A. Clough, 1997: Radiative transfer for inhomogeneous atmospheres: RRTM, a validated correlated-*k* model for the longwave. *J. Geophys. Res.,* **102,** 16 663–16 682.

Noh, Y., W. G. Cheon, S. Y. Hong, and S. Raasch, 2003: Improvement of the *K*-profile model for the planetary boundary layer based on large eddy simulation data. *Bound.-Layer Meteor.,* **107,** 401–427.

Pielke, R. A., Sr., G. Marland, R. A. Betts, T. N. Chase, J. L. Eastman, J. O. Niles, D. S. Niyogi, and S. W. Running, 2002: The influence of land-use change and landscape dynamics on the climate system: Relevance to climate-change policy beyond the radiative effects of greenhouse gases. *Philos. Trans. Roy. Soc. London,* **360A,** 1–15.

Pu, B., E. K. Vizy, and K. H. Cook, 2012: Warm season response over North America to a shutdown of the Atlantic meridional overturning circulation and CO_2 increases. *J. Climate,* **25,** 6701–6720.

Rockel, B., C. L. Castro, R. A. Pielke Sr., H. von Storch, and G. Leoncini, 2008: Dynamical downscaling: Assessment of model system dependent retained and added variability for two different regional climate models. *J. Geophys. Res.,* **113,** D21107, doi:10.1029/2007JD009461.

Sertel, E., A. Robock, and C. Ormecia, 2010: Impacts of land cover data quality on regional climate. *Int. J. Climatol.,* **30,** 1942–1953, doi:10.1002/joc.2036.

Stauffer, D. R., and N. L. Seaman, 1990: Use of four-dimensional data assimilation in a limited-area mesoscale model. Part I: Experiments with synoptic-scale data. *Mon. Wea. Rev.,* **118,** 1250–1277.

Trusilova, K., M. Jung, G. Churkina, U. Karstens, M. Heimann, and M. Claussen, 2008: Urbanization impacts on the climate in Europe: Numerical experiments by the PSU–NCAR Mesoscale Model (MM5). *J. Appl. Meteor. Climatol.,* **47,** 1442–1455.

von Storch, H., 1999: The global and regional climate system. *Anthropogenic Climate Change,* H. von Storch and G. Floser, Eds., Springer-Verlag, 3–36.

——, H. Langenberg, and F. Feser, 2000: A spectral nudging technique for dynamical downscaling purposes. *Mon. Wea. Rev.,* **128,** 3664–3673.

Waldron, K. M., J. Paegle, and J. D. Horel, 1996: Sensitivity of a spectrally filtered and nudged limited-area model to outer model options. *Mon. Wea. Rev.,* **124,** 529–547.

Wang, W., and Coauthors, 2012: Advanced Research WRF (ARW) version 3 modeling system user's guide. Mesoscale and Microscale Meteorology Division, NCAR, 384 pp.

Wigley, T. M. L., P. D. Jones, K. R. Briffa, and G. Smith, 1990: Obtaining sub-gridscale information from coarse-resolution general circulation model output. *J. Geophys. Res.,* **95,** 1943–1953.

Wilby, R. L., T. M. L. Wigley, D. Conway, P. D. Jones, B. C. Hewitson, J. Main, and D. S. Wilks, 1998: Statistical downscaling of general circulation model output: A comparison of methods. *Water Resour. Res.,* **34,** 2995–3008.